Evolution of the broadly rifted zone in southern Ethiopia through gravitational collapse and extension of dynamic topography

Luelseged Emishaw [a], Daniel A. Laó-Dávila [a], Mohamed G. Abdelsalam [a,*], Estella A. Atekwana [a], Stephen S. Gao [b]

[a] Oklahoma State University, Boone Pickens School of Geology, 105 Noble Research Center, Stillwater, OK 74078-3031, United States
[b] Missouri University of Science and Technology, Geology and Geophysics Program, 129 McNutt Hall, Rolla, MO 65409, United States

ABSTRACT

The Broadly Rifted Zone (BRZ) is a ~315 km wide zone of extension in southern Ethiopia. It is located between the Southern Main Ethiopian Rift and the Eastern Branch of the East African Rift System (EARS) represented by the Kenya-Turkana Rift. The BRZ is characterized by NE-trending ridges and valleys superimposed on regionally uplifted (~2 km average elevation) terrain. Previous studies proposed that the BRZ is an overlap zone resulted from northward propagation of the Kenya-Turkana Rift and southward propagation of the Southern Main Ethiopian Rift. To understand the relationship between the BRZ's extensional style and its crustal and upper mantle structures, this work first estimated the Moho depth using the two-dimensional (2D) radially-averaged power spectral analysis of the World Gravity Map. Verification of these results was accomplished through lithospheric-scale 2D forward gravity models along E-W profiles. This work found that the Moho topography beneath the BRZ depicts a dome-like shape with a minimum depth of ~27 km in the center of the dome. This work proposes that the Moho doming, crustal arching underlying the BRZ and associated topographic uplift are the result of asthenospheric mantle upwelling beneath the BRZ. This upwelling changed to a NE-directed lateral mantle flow at shallower depth. This is supported by seismic tomography imaging which shows slow S-wave velocity anomaly at lithospheric depth of 75 km to 150 km stretching in a NE-SW direction from beneath the BRZ to the Afar Depression. This work proposes that the asthenospheric upwelling created gravitationally unstable dynamic topography that triggered extensional gravitational collapse leading to the formation of the BRZ as a wide rift within the narrow rift segments of the EARS.

1. Introduction

Narrow rifts as exemplified by the majority of the segments of the East African Rift System (EARS) are less than 100 km in width (Fig. 1). They generally develop where the localization of the extensional strain is facilitated by the presence of mechanical and/or thermal weaknesses such as lithospheric-scale heterogeneities and/or intrusion of magmatic bodies (e.g. Ebinger and Casey, 2001; Chorowicz, 2005). These rifts are typically underlain by thinned crust and sub-continental lithospheric mantle (SCLM) where thinning is restricted to a narrow and linear zone that follows the surface expression of the rift basin. For example, from reflection/refraction seismic profile across the Main Ethiopian Rift (Fig. 1) MacKenzie et al. (2005) observed slight crustal thinning beneath the rift. Additionally, MacKenzie et al. (2005) observed faster seismic velocity in the upper crust beneath the rift and attributed this to the presence of mafic intrusions. Also, from passive seismic receiver function study, Stuart et al. (2006) found that the crust beneath the Main

Ethiopian Rift becomes progressively thinner towards the north ranging from 38 km in the south to 30 km in the north. Stuart et al. (2006) also found higher Poisson's ratio within the crust beneath the rift and interpreted this to indicate the presence of partial melting. Besides documenting thinning of the crust beneath the Main Ethiopian Rift, Dugda et al. (2007) used joint inversion of seismic Rayleigh wave group velocities and receiver function to show that the SCLM beneath the rift is also thinner reaching only ~50 km thickness compared to the 100–150 thickness of the SCLM in regions that are not affected by rifting.

Additionally, Tiberi et al. (2005) used the inversion of gravity data constrained by previous results from passive seismic receiver function studies to image crustal and upper mantle structure beneath the Main Ethiopian Rift, the Afar Depression and the Ethiopian Plateau (Fig. 1). Tiberi et al. (2005) found that crustal thickness decreases from 33 km along the axis of the Main Ethiopian Rift in the south to 24 km in the southern part of the Afar Depression. Also, Tiberi et al. (2005) found the crust to be thicker beneath the Ethiopian Plateau reaching ~40 km. Further, Tiberi et al. (2005) attributed the presence of denser crust beneath much of the Ethiopian Plateau and portions of the Main Ethiopian Rift to magmatic under-plating.
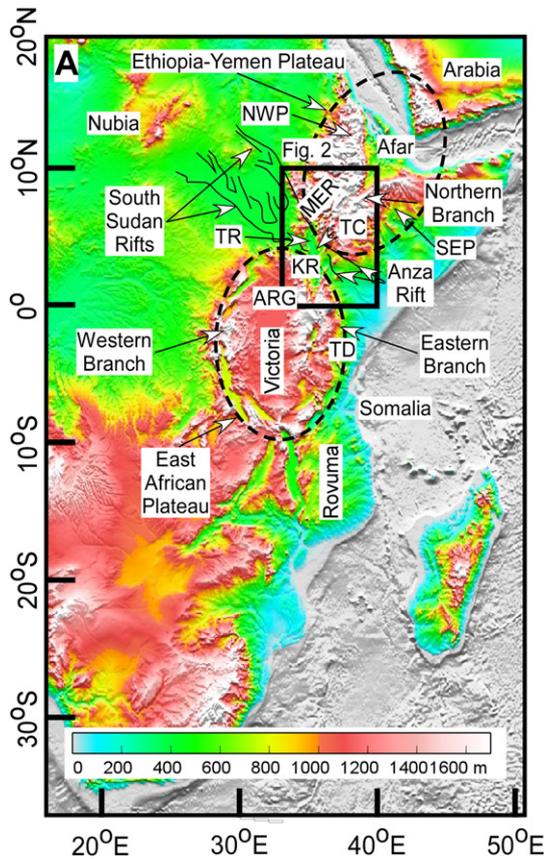
Fig. 1. Global Topographic 30 arc second (GTOPO30) Digital Elevation Model (DEM) showing the East African Rift System (EARS). MER = Main Ethiopian Rift. NWP = Northwestern Ethiopian Plateau. SEP = Southeastern Ethiopian Plateau. TR = Turkana Rift. KR = Kenya Rift. TC = Turkana Topographic Corridor. ARG = Albertine-Rhino Graben. TD = Tanzania Divergence Zone.

Fig. 2. Shuttle Radar Topography Mission (SRTM) Digital Elevation Model (DEM) showing the location of the Broadly Rifted Zone (BRZ) between the Southern Main Ethiopian Rift and the northern continuation of the Kenya-Turkana Rift represented by Omo Basin.

The surface and upper crustal structures of narrow continental rifts are characterized by the presence of curvilinear and high-angle border faults that accommodate extension and control the subsidence in the basins during the early stages of rifting, often through the development of half-grabens with along-strike alternation and change of half-graben polarity (e.g. Ebinger and Casey, 2001).

The EARS (Fig. 1) constitutes rift segments that are 70–100 km wide and form asymmetric rift basins flanked by steep normal faults (Chorowicz, 2005). This rift system can be divided into Northern, Eastern and Western Branches (Fig. 1). The Northern Branch stretches within Ethiopia, Eritrea and Djibouti and it constitutes the Afar Depression in the north and the Main Ethiopian Rift to the south (Fig. 1). The Main Ethiopian Rift in turn is divided into Northern, Central and Southern segments (Fig. 2; Abebe et al., 2007; Corti, 2009). The Southern Main Ethiopian Rift widens further south into a ~315 km zone of diffused extension. This zone is referred to as the Broadly Rifted Zone (BRZ) (Fig. 2; Cerling and Powers, 1977; Moore and Davidson, 1978; WoldeGabriel and Aronson, 1987, 1991; Ebinger et al., 1993, 2000; Bonini et al., 2005; Philippon et al., 2014). The BRZ is also referred to as the Basin and Range of Ethiopia (Moore and Davidson, 1978; Corti, 2009). South of the BRZ, the EARS extends as the Eastern Branch which is represented by the ~70 km wide Turkana Rift in the north, the Kenya Rift in the center, and the Tanzania Divergence Zone to the south (Fig. 1; Ebinger et al., 2000).

The BRZ consists of a number of basins that form a Basin and Range type topography (Figs. 2 and 3; Moore and Davidson, 1978; Ebinger et al., 2000; Corti, 2009). This topography resulted from the presence of tilted blocks of Eocene-Pliocene volcanic rocks bounded by steep normal faults forming asymmetrical grabens or half-grabens. The tilted
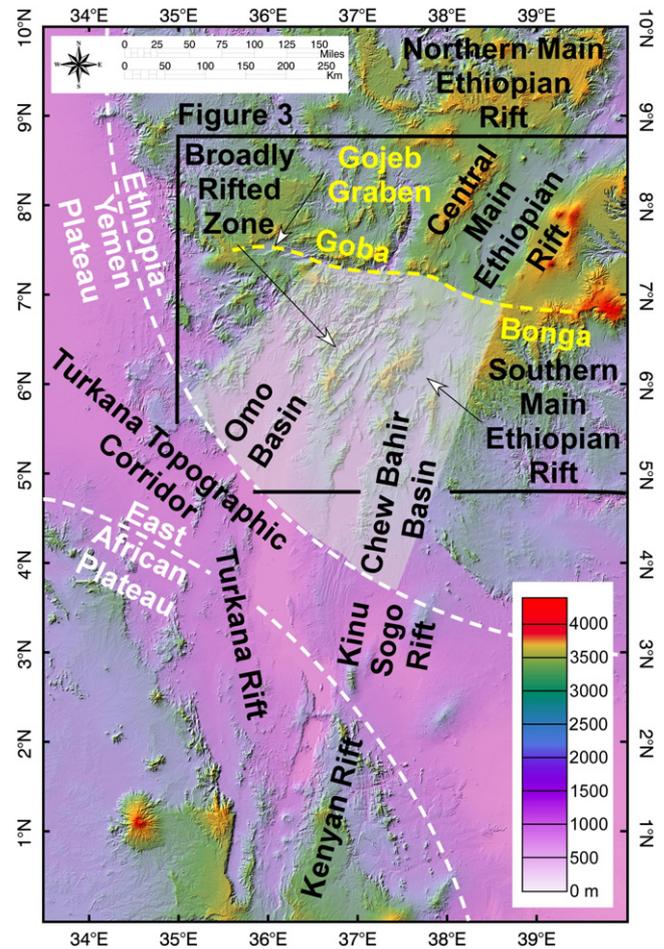
blocks rest unconformably on Precambrian crystalline basement and the half-grabens are filled with Miocene-Pliocene sedimentary rocks (Figs. 4 and 5). Ebinger et al. (1993, 2000) suggested that the structural characteristics of the BRZ are typical of those found in narrow rift basins. Additionally, although the Precambrian crystalline basement rocks (typically amphibolite metamorphic facies gneisses and migmatites which are indicative of middle crustal level of metamorphism) are exposed in many places on the surface (Fig. 4), no low-angle detachment faults or metamorphic core complexes are observed within the BRZ. These observations suggest that the BRZ developed through processes different from those suggested for wide rifts such as the Basin and Range of the western United States.

Results from remote sensing, structural geology, geomorphological, and geochronological studies were used to suggest that the BRZ is an overlap zone between the Southern Main Ethiopian Rift and the Kenya-Turkana Rift (Fig. 2). In addition, the development of individual basins constituting the BRZ was explained as due to eastward migrating of the Kenya-Turkana Rift during its northward propagation, as well as the southward propagation of the Southern Main Ethiopian Rift (Cerling and Powers, 1977; Moore and Davidson, 1978; WoldeGabriel and Aronson, 1987; Ebinger et al., 2000; Bonini et al., 2005; Philippon et al., 2014). Further, poly-phase oblique rifting and anti-clockwise rotation have been proposed as factors that might have contributed to the widening of the BRZ (Boccaletti et al., 1998; Bonini et al., 2005; Corti, 2009; Philippon et al., 2014).

This study used two-dimensional (2D) radially-averaged power spectral analysis of the World Gravity Map (WGM 2012) to image the depth to Moho beneath the BRZ and its surroundings. Also, this work
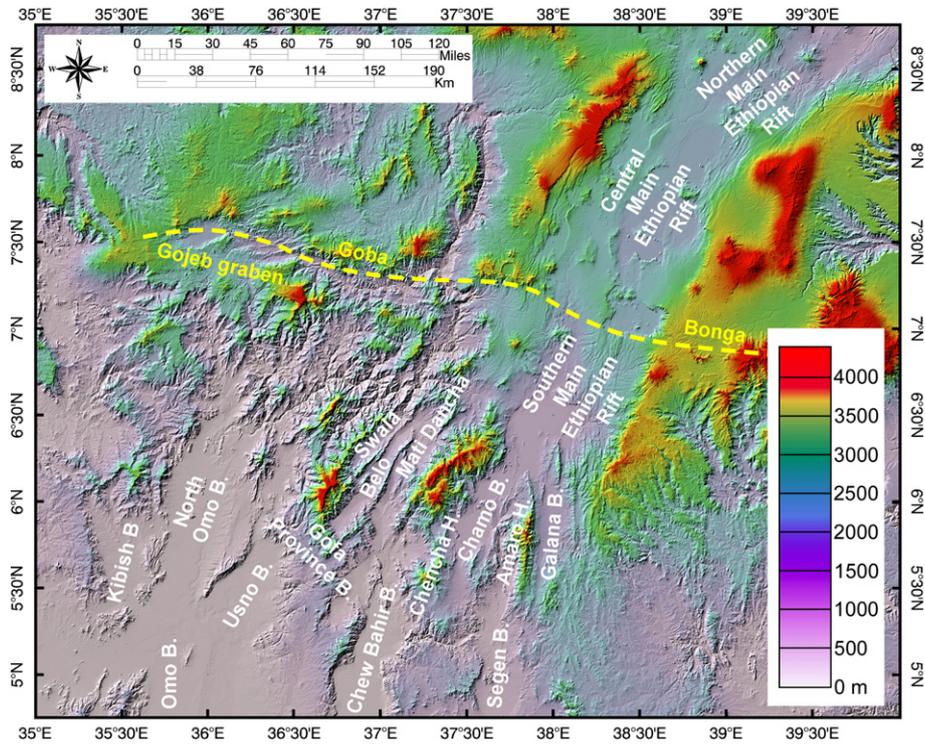
Fig. 3. Shuttle Radar Topography Mission (SRTM) Digital Elevation Model (DEM) showing the rift basins constituting the Broadly Rifted Zone (BRZ) in southern Ethiopia.

developed 2D forward gravity models from the WGM 2012 to construct E-W trending lithospheric-scale sections across the BRZ and the Central Main Ethiopian Rift. The 2D forward gravity models were used to verify the Moho depth estimates from the 2D radially-averaged power spectral analysis and to compare lithospheric structure of the narrow rift in the north with that of the BRZ. This study also used various horizontal depth slices of S-wave seismic tomography from Grand (2002) and

Fishwick (2010) models to understand deeper lithospheric and asthenospheric structures beneath the BRZ and its surroundings. The aim of this work was to explore any relationship between the geometry of the BRZ and its surface topographic expression on the one hand and deeper features including the Moho depth and deeper lithospheric and asthenospheric structures on the other hand that might lead to better explanation of its geodynamic development.
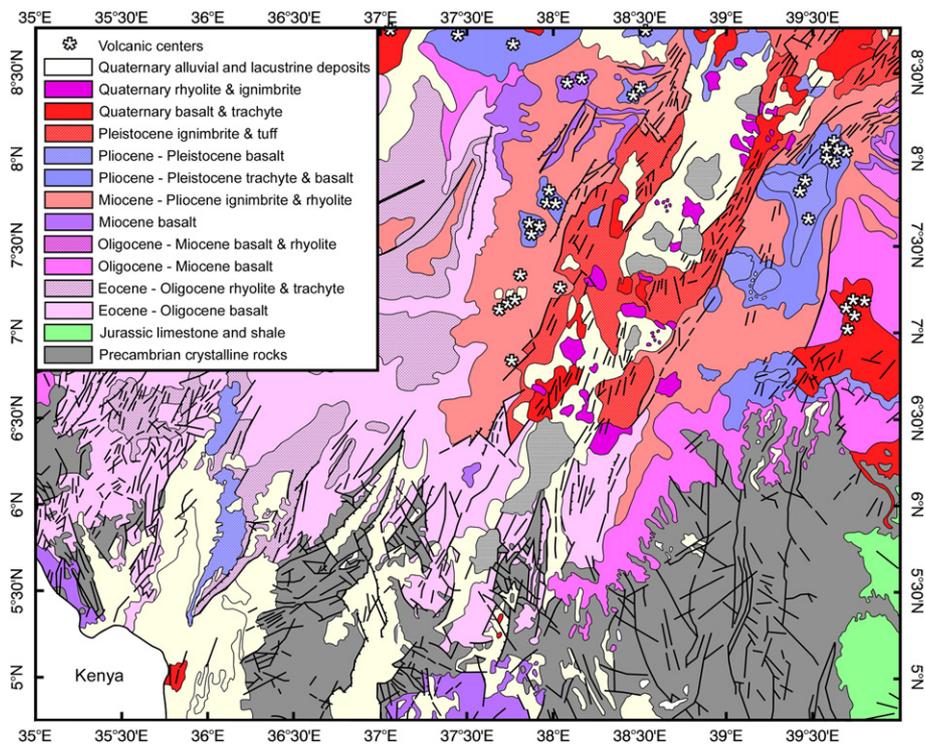

Fig. 4. Geological map of the Broadly Rifted Zone (BRZ) and its surroundings modified from the geological map of Ethiopia (Mengesha et al., 1996).
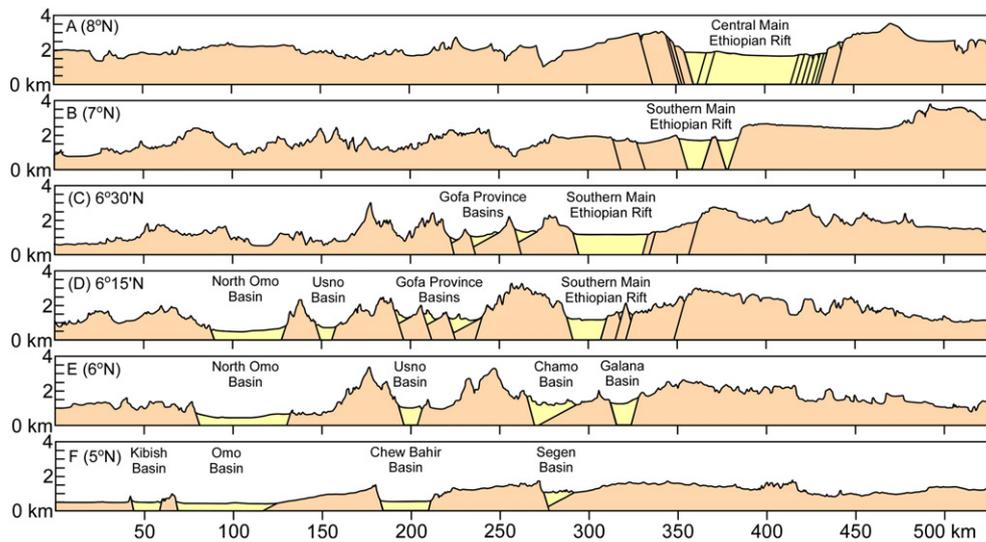
Fig. 5. Idealized **E**-W sections across: (A) Central Main Ethiopian Rift. (B) Southern Main Ethiopian Rift. (C) Southern Main Ethiopian Rift and the northern part of the Gofa Province Basins. (D) The Southern Main Ethiopian Rift, the central part of the Gofa Province Basins and the northern extension of the Omo Basin (North Omo and Usno basins). (E) The Southern Main Ethiopian Rift (Chamo and Galana basins) and the Omo Basin (North Omo and Usno basins). (F) Basins in the southern part of the Broadly Rifted Zone (BRZ) (Kibish, Omo, Chew Bahir, and Segen basins).

2. Tectonic setting

2.1. The East African Rift System

The EARS is a complex extensional regime between the Nubia, Somalia, and Arabia plates in its northern part, and between the Nubia, Somalia, Victoria and Rovuma plates in its southern part (Fig. 1; Saria et al., 2014). It can be divided into three main branches. First, the Northern Branch that constitutes the Afar Depression and the Main Ethiopian Rift. Second, the Eastern Branch that constitutes the Turkana Rift, the Kenya Rifts and the Tanzania Divergence Zone. Third, the Western Branch that extends southward from the Rhino-Albertine Graben (Fig. 1; Chu and Gordon, 1999; Chorowicz, 2005). Morphologically, the Northern Branch is associated with the dynamic topography of the Ethiopia-Yemen Plateau whereas the Eastern and Western Branches are associated with the dynamic topography of the East African Plateau (Fig. 1). The two plateaus are separated by the Turkana Topographic Corridor (Fig. 1). The origin of the two plateaus was linked to upwelling of a single mantle plume beneath the stationary African Plate with lateral flow and ponding (Ebinger and Sleep, 1998) or upwelling of two distinct mantle plumes referred to as the Afar and Kenya plumes (Rogers et al., 2000). Differently, Moucha and Forte (2011) interpreted the dynamic topography of the Ethiopia-Yemen and East African plateaus as due to northward movement of the African Plate above the upwelling African Super Plume.

2.2. The Broadly Rifted Zone (BRZ)

The BRZ includes rifts from the Northern Branch (Southern Main Ethiopian Rift), the Eastern Branch (the Kenya-Turkana Rift) and the overlap zone between them (Figs. 2 and 3). This work focuses on the Ethiopian part of the BRZ. It defines the BRZ as constituting the Southern Main Ethiopian Rift basins in the east, the Gofa Province Basins in the center, and the Kenya-Turkana Rift basins to the west. This work also considers the BRZ basins to be bounded in the north by the Goba-Bonga lineament (Bonini et al., 2005) and these basins extend to the south until the northeastern margin of the Turkana Topographic Corridor (Fig. 2). The Goba-Bonga lineament, although lacking continuous structural and morphological expression, has been proposed for a number of factors (Bonini et al., 2005). (1) The western part of it coincides with the E-W trending Gojeb Graben (Figs. 2 and 3). (2) The border

faults of the Main Ethiopian Rift rotate slightly from N20°E – N35°E north of the lineament (the Central Main Ethiopian Rift) to N5°E – N20°E south of the lineament (the Southern Main Ethiopian Rift) (Fig. 2). (3) The Gofa Province Basins do not continue north of the lineament (Fig. 3).

The Southern Main Ethiopian Rift narrows slightly south of the Goba-Bonga lineament compared to the Central Main Ethiopian Rift (Figs. 3 and 5A–D). It bifurcates further south into the Chamo and Galana basins separated by the Amaro Horst (Figs. 3 and 5E; Levitte et al., 1974). Further south, the Chamo and Galana basins give place to the Segen Basin (Figs. 3 and 5F). Hayward and Ebinger (1996) and Ebinger and Hayward (1996) showed that the basins constituting the Southern Main Ethiopian Rift are 50 to 100 km long and 30 to 65 km wide.

The Kenya Rift extends northward into the Turkana Rift, which in turns continues northward as the Omo Basin (Fig. 2). Further north, the Omo basin bifurcates into the Kibish, the Usno and the Northern Omo basins (Figs. 3, 5E and F). Vetel and LeGall (2006) suggested that the Turkana magmatic rift is ~200 km wide and was initiated ~45 Ma within the NW-trending Mesozoic rifts of South Sudan and the Anza Rift in northern Kenya (Fig. 1). Further, Vetel and LeGall (2006) proposed that the evolution of the Turkana Rift is influenced by Precambrian basement faults and softening of the crust by magmatic injection. From structural observations and gravity analysis, Mammo (2012) showed that the Omo Basin is an asymmetrical half-graben bounded by N-S to NNE-SSW early Pliocene border faults. Mammo (2012) also showed that the basin is filled with over 4 km of sediments.

A segment of the Kenya Rift branches off and continues north into the Kinu Sogo Rift which crops out within the Turkana Topographic Corridor (Fig. 2; Vetel et al., 2005). The Kinu Sogo Rift in turn continues north into the Chew Bahir Basin (Fig. 2). The Chew Bahir Basin is separated from the Chamo Basin by the Chencha Host (Fig. 3). Vetel et al. (2005) described the Kinu Sogo Rift as ~40 km wide extensional structure that comprises a number of narrow, N-trending horsts and grabens (Fig. 2) that dissect Miocene – Pliocene lavas. Further, Vetel et al. (2005) showed that the average displacement on the individual fault segments that are ~9 km long is not more than 100 m. Vetel et al. (2005) attributed this significantly low displacement to fault length ratio to strong influence of reactivation of pre-existing structures or fractures that were formed in association with the extrusion and crystallization of the lava.

The Southern Main Ethiopia Rift and the Kenya-Turkana Rift basins enclose the Gofa Province Basins, which represent the central part of the BRZ in Ethiopia (Figs. 3 and 5D). The Gofa Province Basins constitute three 10–15 km wide half-grabens represented by, from east to west, the Mati Dancha, Bet and Swala basins (Fig. 3; Philippon et al., 2014). The Mati Dancha Basin extends southward into the Chew Bahir Basin (Fig. 3). The half-grabens of the Gofa Province Basins are thought to have been formed by oblique rifting whereas the eastern (Galana Basin) and western (North Omo Basin) basins of the BRZ are interpreted to be the result of the northward propagation of the Kenya-Turkana Rift and the southward propagation of the Southern Main Ethiopian Rift (Ebinger et al., 2000; Corti et al., 2009).

The presence of mostly NE-trending individual basins makes the BRZ ~315 km wide in an E-W direction. These basins are mainly bounded by steeply-dipping faults. Bio-geochronological studies as well as radiogenic and cosmogenic age dating suggest that these faults started developing as early as Early to Middle Miocene, especially in the Southern Main Ethiopian Rift, the Gofa Province Basins and the Chew Bahir Basin (WoldeGabriel et al., 1991; Ebinger et al., 1993, 2000). Ebinger et al. (1993, 2000) reported that extension was accompanied by volcanic activities dated at 20–11 Ma. Additionally, Bonini et al. (2005) reported a K/Ar age of ~20 Ma from a basaltic dike on the flanks of the Chencha Horst north of the Chew Bahir Basin (Fig. 3). Pik et al. (2008) reported a (U/Th)He age of ~20 Ma from the Chew Bahir Basin and this has been taken as the onset age of the extension. Corti et al. (2013) and Philippon et al. (2014) used ^{14}C age dating of smeared organic matter on border fault planes from the Southern Main Ethiopian Rift and the Chamo Basin to suggest the presence of faulting activities younger than 30 ka. Additionally, Philippon et al. (2014) used apatite fission track age dating of Precambrian crystalline rocks from the Gofa Province Basins (Figs. 3 and 4) to report ages between ~11 and 7 Ma. Philippon et al. (2014) explained this geochronological data as indicating the age of exhumation of the Precambrian crystalline basement rocks. Further, Philippon et al. (2014) suggested that the young ages obtained in the Gofa Province Basins compared to those obtained by Pik et al. (2008) from the Chew Bahir Basin (Figs. 3 and 4) indicate northward propagation of the Kenya-Turkana Rift. Balestrieri et al. (2016) obtained apatite fission track ages of 12.3 ± 2.7 Ma and 6.8 ± 0.7 Ma from samples collected from the Precambrian crystalline basement rocks exposed in the Amaro Horst and 22.8 ± 3.3 Ma and 7.0 ± 0.7 Ma for samples from the Precambrian crystalline basement rocks exposed within the Beto Basin of the Gofa Province Basins (Figs. 3 and 4). Balestrieri et al. (2016) concluded from thermal modeling that exhumation of the Precambrian crystalline basement rocks started at 12 ± 2 Ma in the Beto Basin and between 10 and 8 Ma in the Amaro Horst.

Results of fault kinematic analysis conducted near the Chencha Horst (Fig. 3) suggest four extensional events. The first extension was in a NNE-SSW direction and was followed by an E-W directed extension as indicated by the presence of slickenlines contained within fault planes superimposed on the previous extensional structures (Bonini et al., 2005). The third phase of extension was in a NW-SE direction while the fourth and the last phase, which is suggested to be Quaternary in age, was in an E-W direction (Bonini et al., 2005). However, focal mechanism fault plane solutions show dominant WNW-ESE directed present-day regional extension (Ebinger et al., 2000), which is suggested to be the result of clockwise rotation of the Somali Plate relative to the Nubia Plate (Bonini et al., 2005).

2.3. The role of pre-existing structures in the evolution of the Broadly Rifted Zone (BRZ)

There are several opinions regarding the relationship between the BRZ and the Precambrian structures of the crystalline basement. For example, Moore and Davidson (1978) observed that there is an apparent parallelism between the faults associated with the BRZ and the Precambrian metamorphic foliation and mylonite zones within the gneissic terrain of southern Ethiopia. Additionally, Moore and Davidson (1978) suggested that the arcuate pattern of the Gofa Province Basins and the zig-zag shape of the western edge of the Chow Bahir Basin (Fig. 3) might have resulted from the presence of regional variation in the trends of the Precambrian structures. Ebinger et al. (2000), however argued that there is little evidence for reactivation of the low-angle gneissic foliations in the Precambrian crystalline basement throughout the development of the BRZ.

This work observes from SRTM DEM that the western border faults of the Chamo and Segen basins and both the eastern and western border faults of the Chew Bahir Basin are characterized by a zig-zag pattern in which the orientations of the border faults alternate between northwest and northeast (Fig. 3). Also, it is observed that the southwestern ends of the NE-trending Beto and Mati Dancha Basins of the Gofa Province Basins are marked by NW-trending faults, almost orthogonal to the general NE-trending faults delimiting these half-grabens (Fig. 3). Differently, no zig-zag pattern is observed in the border faults of the N-trending Galana Basin (Fig. 3). The NW-trending faults of the Chamo, Segan and Chew Bahir basins as well as the southwestern ends of the Beto and Mati Dancha of the Gofa Province Basins seem to follow pre-existing Precambrian structures as indicated by the parallelism between the morphological expression of these faults and closely-spaced lineaments observed in the SRTM DEM (Fig. 3). Similarly, the N-trending border faults of the Galana Basin appear to follow pre-existing Precambrian structures (Fig. 3). However, the NE-trending border faults of the Chamo, Segan and Chew Bahir basins as well as the Beto and Mati Dancha of the Gofa Province Basins do not follow any Precambrian structures and cut almost orthogonal to them (Fig. 3).

South of the BRZ in Ethiopia, the Turkana Rift is exposed within the Turkana Topographic Corridor (Fig. 2). The region to the northwest of this topographic low hosts the Mesozoic rifts of South Sudan (Fig. 1). Similarly, the Mesozoic Anza Rift in northern Kenya is found to the southeast of the Turkana Topographic Corridor (Fig. 1). Hendrie et al. (1994) concluded from gravity and seismic studies that the South Sudan Rifts and the Anza Rift were connected during the Paleogene. Hendrie et al. (1994) proposed that the EARS reactivated some of these basins during the Neogene. Additionally, Hendrie et al. (1994) showed that the crust beneath the Turkana Topographic Corridor is only 20 km thick and attributed some of this thinning to extension prior to the formation of the EARS.

3. Data and methods

3.1. World Gravity Map (WGM 2012)

The World Gravity Map (WGM 2012) (Fig. 6) was used in this study. The WGM 2012 is a gravity anomaly map that is produced from three components: (1) the United States National Geospatial Intelligence Agency's Earth Gravity Model (EGM 2008); (2) the Denmark's National Space Institute, Denmark Technical University (DTU 10) global gravity field model; and (3) elevation data of the Global Topographic 30 arc second (GTOPO30) global relief model (Bonvalot et al., 2012). The EGM 2008 model was developed from two components: (1) the global set of area-mean free-air gravity anomalies defined on a 5 arc-minute equiangular grid. This includes terrestrial, altimetry-derived, and airborne gravity data; and (2) the least squares combination of the Spain's Instituto Tecnológico de Galicia Gravity Recovery and Climate Experiment (ITG-GRACE03S) gravitational field model. This consists of the static high resolution model, the full variance-covariance matrix, the temporal variation, and the associated error covariance matrix.

3.2. Two-dimensional (2D) radially-averaged power spectrum analysis

Spectral analysis of gravity data to estimate the Moho depth relies on the Fourier transformation. The principle of this transformation is that any function in time or space domain can be represented by an equal
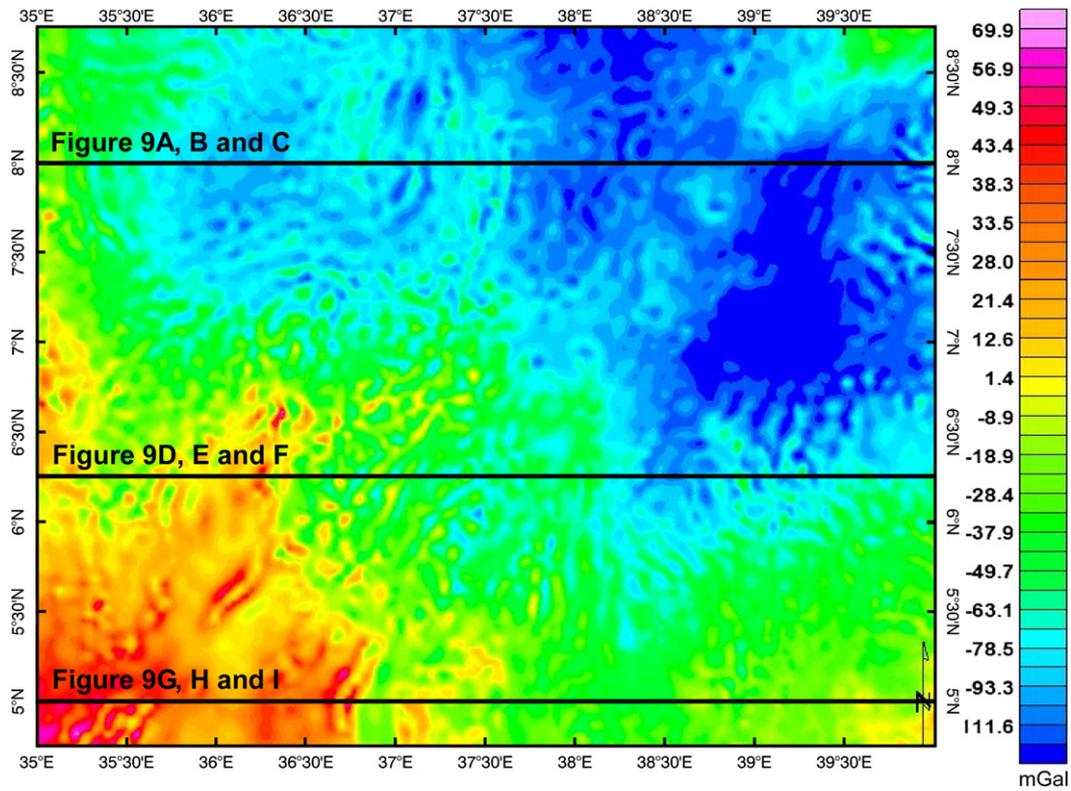
Fig. 6. The Bouguer gravity anomaly map of the World Gravity Map (WGM2012) used for the estimation of Moho depth beneath the Broadly Rifted Zone (BRZ) using two-dimensional (2D) radially-averaged power spectral analysis and 2D forward modeling. Solid horizontal black lines represent the baselines of the two-dimensional (2D) forward gravity models shown in Fig. 9.

number of sinusoidal function-frequency domain. The power spectrum of a frequency domain is represented by the equation:

$$P_h(r) = e^{-2hr}P_0(r) \tag{1}$$

where "$P_h(r)$" is the power spectrum of the top gravity surface "$P_0(r)$" and "r" is the wavenumber. The representation of this formula in the linear equation is expressed as:

$$\ln P_h(r) = -2hr + c \tag{2}$$

where "h" is the slope of the spectral curve and "c" is a constant. The log plots of "Ln_P" versus wavenumber results in the power spectrum graph from which the depth to the source can be estimated (Tselentis et al., 1988). The depth to the Moho can be estimated from the middle slope of the 2D radially-averaged spectral curve (Tselentis et al., 1988) as shown in Fig. 7. This work used the middle slope of the spectral curve corresponding to wavenumber ranging between 0.14 and 0.26 cycles/km. This is because the middle section of the spectral curve has a distinctive slope that is different from its steeper upper part and the shallower lower part (Fig. 7).

The 2D radially-averaged power spectral curves were computed from 1° × 1° windows (~110 km × 110 km) of the WGM 2012 covering the BRZ and its surroundings with 50% N-S and **E-**W overlap between the windows. Two hundred and twenty one curves corresponding to the 1° × 1° windows were produced covering an area of 316,350 km² within and around the BRZ. The Oasis Montaj MagMap software was used to produce the 2D radially-averaged power spectral curves. These curves were then plotted in the Office-Excel Spreadsheet to calculate the middle slope of the spectral curves. This was achieved by using the LINEST equation that computes slope from the known X's and Y's values of any exponential to linear curves. This equation was also used

to determine the statistical fit of the middle slope of the spectral curves against the original X-Y plot.

The 1° × 1° window size is selected because it shows the steeper, the shallower and the middle spectral wavenumber components of the spectral curve without exaggerated overlaps. Smaller window sizes, such as 0.5° × 0.5°, only show overlapped deeper and shallower spectral components on the spectral curve and therefore are incapable of distinctly determining the Moho depth. Larger window sizes could potentially mix-up the spectral wavenumbers and lead to the overestimation of the derived Moho depth. The 50% E-W and N-S overlaps are used to
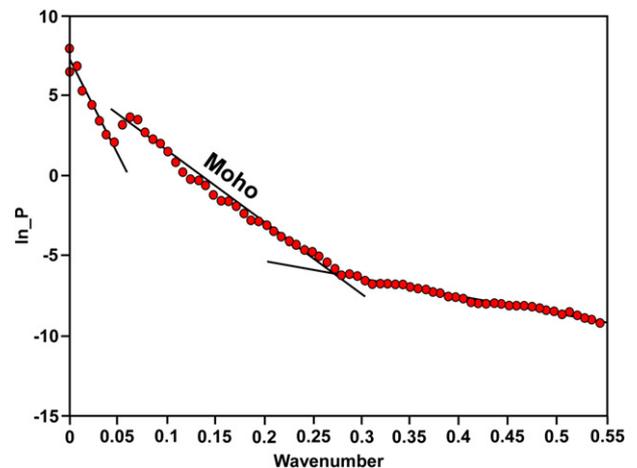

Fig. 7. An example of two-dimensional (2D) radially-averaged power spectral curve computed from the World Gravity Map (WGM2012) for a 1° × 1° (~110 km × 110 km) window.

reduce the Gibbs phenomena where the boundaries of the sub-regions behave as jump discontinuities (Leseane et al., 2015).

3.3. Two-dimensional (2D) forward gravity modeling

To verify the Moho depth results obtained from the 2D radially-averaged power spectral analysis and to compare the cross-sectional view of the lithospheric structure of the BRZ with extensional structures to the north of it, three 2D forward gravity models were constructed from the WGM 2012. These models are along latitudes 8° N (crossing the Central Main Ethiopian Rift), 6° 15′ N (crossing the central part of the BRZ), and 5° N (crossing the southern part of the BRZ). The three 2D forward gravity models extend between longitudes 35° E and 40° E (Fig. 6). These models were developed using the 2D GYMSYS Oasis Montaj software. The software is based on Talwani et al. (1959) which was later reformatted by Won and Bevis (1987) for better computational efficiency. A density value of 2.60 g/cm^3 was assigned to the upper crust, 2.85 g/cm^3 to the lower crust, and 3.10 g/cm^3 to the SCLM. A density value of 2.40 g/cm^3 was assigned to the sedimentary rocks filling the rift basins.

This work used the depth to Moho obtained from the 2D radially-averaged power spectral analysis as an initial constraint for the 2D forward gravity modeling of the WGM 2012. Further, to reduce the number of possible solutions, this work calculated the sensitivity of the models to changes in the density values of the upper crust, lower crust and the SCLM. The sensitivity was determined by assigning geologically acceptable minimum and maximum density values for each layer. These are 2.60 to 2.74 g/cm^3 for the upper crust, 2.80 to 3.02 g/cm^3 for the lower crust, and 3.00 to 3.33 g/cm^3 for the SCLM.

4. Results

4.1. Moho depth estimation from the two-dimensional (2D) radially-averaged power spectral analysis

The Moho depth map of the BRZ and its surroundings (Fig. 8A) shows a significant variation in the crustal thickness that ranges between 27 and 43.5 km. In order to compare the Moho depth variation with the surface morphological expression of the BRZ and its surroundings, a transparent version of the Moho depth image was draped onto a grey-scale DEM extracted from the SRTM data (Fig. 8B). The merged image of the Moho depth and the SRTM DEM shows both the Moho depth variation and the surface morphology and structure of the BRZ and its surroundings in a single image (Fig. 9B).

The Main Ethiopian Rift shows different Moho depth values beneath each of its three segments. The Moho beneath the Northern Main Ethiopian Rift is ~34 km deep, and deepens beneath the Central Main Ethiopian Rift to ~38 km. The depth to Moho beneath the Southern Main Ethiopian Rift is ~32 km (Fig. 8B). The Moho depth beneath the Somali Plateau ranges between 39 and 43 km and the plateau shows a relatively uniform crustal thickness (Fig. 8B). Differently, the Ethiopian Plateau shows heterogeneous crustal thickness in which the relatively shallower Moho depth ranges between 40 and 43 km.

Beneath the Gofa Province Basins which represent the central part of the BRZ, the Moho depth becomes shallower reaching a depth of ~27.5 km (Fig. 8B). There is a gradual Moho depth increase from the Gofa Province Basins towards the Northwestern and Southeastern Ethiopian plateaus in which the depth to the Moho reaches 43.5 km (Fig. 8B). Beneath the Gofa Province Basins, the shallow Moho anomaly forms a circular feature in map view that is 210 km wide in the E-W direction and 240 km wide in the N-S direction (Fig. 8B). The Moho is shallowest in the central part of this circular feature and becomes progressively deeper away from the center suggesting that the three-dimensional (3D) topography of the Moho beneath the Gofa Province Basins depicts a domical geometry.

The results of the Moho depth estimates from the 2D radially-averaged power spectral analysis are generally consistent with the Moho depth estimated from previous passive seismic studies by Dugda et al. (2005) and Keranen et al. (2009) (Table 1; Fig. 8A). The root mean square error (RMSE) was calculated to quantify the cumulative discrepancy in the Moho depth results of this work and those of Dudga et al. (2005) and Keranen et al. (2009). The RMSE between the Moho depth estimates from the 2D radially-averaged power spectral analysis and those from Dugda et al. (2005) and Keranen et al. (2009) is calculated as ~5.0 km and ~3.1 km, respectively. The difference between the Moho depth estimates obtained in this study and those of Dugda et al. (2005) is equal or less than ± 5.0 km in 9 of the 11 stations used in the calculations of the RMSE (Table 1). The largest difference in the Moho depth estimates between the two studies came from stations NAZA and SELA where differences of 9.5 and 11.5 km were respectively found. The Moho depth estimates obtained by Dugda et al. (2005) also show large differences with Moho depth calculated by Keranen et al. (2009) for these two stations. Dugda et al. (2005) estimated the Moho depth to be 27.0 km in stations NAZA and SELA while Keranen et al. (2009) found it to be 35.5 km and 40.5 km, respectively (Table 1). Removing these two stations from the RMSE calculation will reduce it to ~2.5 km between the Moho depth estimates from the 2D radially-averaged power spectral analysis and those obtained by Dugda et al. (2005) from passive seismic analysis.

The broadband passive seismic stations used in the Moho depth estimation cover predominantly the Main Ethiopian Rift and the Southeastern Ethiopian Plateau (Fig. 8A). However, both Dugda et al. (2005) and Keranen et al. (2009) reported results from three stations close to the northeastern and eastern margin of what have been identified in this work as the dome-shaped elevated Moho (stations JIMA, TERC, and ARBA in Table 1 and Fig. 8A). In these stations, Dugda et al. (2005) reported Moho depth of 36.0 km, 34.0 km, and 30 km while Keranen et al. (2009) reported Moho depths of 35.5 km, 33.0 km, and 28.0 km, respectively. These estimates compare well with the 33.5 km, 34.0 km, and 32.5 km Moho depth estimates obtained from the 2D radially-averaged power spectral analysis (Table 1).

4.2. Results from the two-dimensional (2D) forward gravity models

The 2D forward gravity models constructed across the Central Main Ethiopian Rift, and the central and southern parts of the BRZ show a number of features associated with the Moho depth. The 2D forward gravity model in Fig. 9C shows a slight shallowing (from ~42 km to ~38 km) of the Moho beneath the Central Main Ethiopian Rift. Differently, there is a more significant shallowing of the Moho beneath the central part of the BRZ from ~40 km to ~30 km (Fig. 9F). This Moho shallowing is centered beneath the long wavelength topographic doming associated with the BRZ (Pink dashed line in Fig. 9E). Also, the 2D forward model suggests necking of the lower crust beneath the BRZ (Fig. 9F). This might be due to ductile flow of the lower crust during extension. The 2D forward model shows a slight and broad shallowing of the Moho beneath the southern part of the BRZ from ~42 km to ~39 km (Fig. 9I).

The 2D forward gravity model along latitude 8° N (Central Main Ethiopian Rift; Fig. 9A and C) shows low sensitivity level to density variation except at its far eastern end where changing the densities of the upper and lower crust results in a relatively low to medium sensitivity level (Fig. 10A). Changing the density of the upper and lower crust from the lower limit (2.60 g/cm^3 for the upper crust and 2.80 g/cm^3 for the lower crust) to the upper limit (2.74 g/cm^3 for the upper crust and 3.02 g/cm^3 for the lower crust) results in changing the calculated gravity anomaly from ~−21 mGal to ~−35 mGal for the upper crust and from ~−38 mGal to ~−70 mGal for the lower crust. This work, thus, gave a special attention to these layers while constructing the 2D forward gravity model.
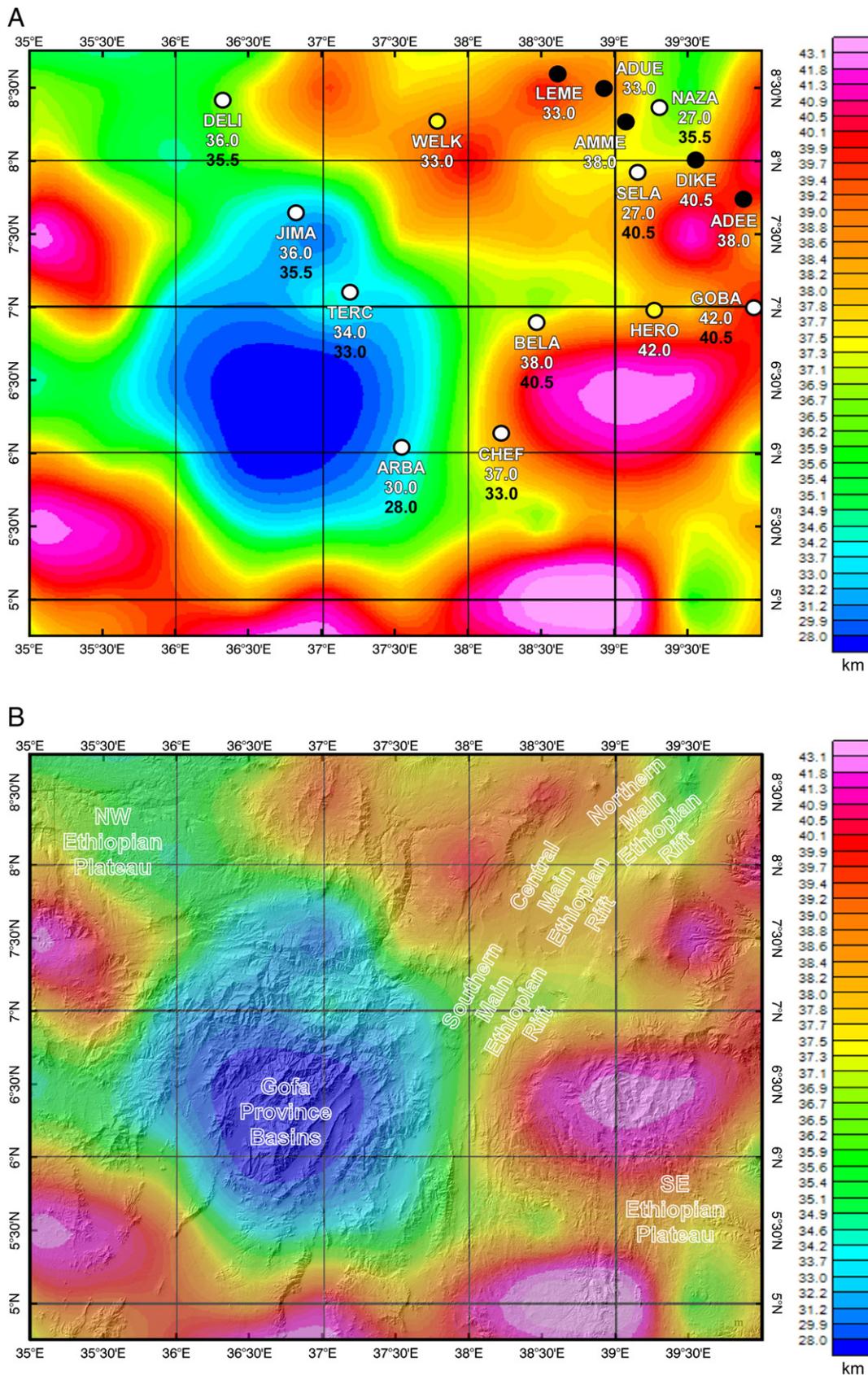
Fig. 8. (A) Moho depth map of the Broadly Rifted Zone (BRZ) and its surroundings constructed from the two-dimensional (2D) radially-averaged power spectral analysis of the World Gravity Map (WGM2012). White circles represent the location, name and Moho depth in km of passive seismic broadband stations results presented by both Dugda et al. (2005; numbers in white) and Keranen et al. (2009; numbers in black). Yellow circles represent the location, name and Moho depth in km of passive seismic broadband stations results presented by Dugda et al. (2005). Black circles represent the location, name and Moho depth in km of passive seismic broadband stations results presented by Keranen et al. (2009). (B) Draping of a transparent version of the Moho depth map in Fig. 9A onto greyscale hillshade Shuttle Radar Topography Mission (SRTM) Digital Elevation Model (DEM).
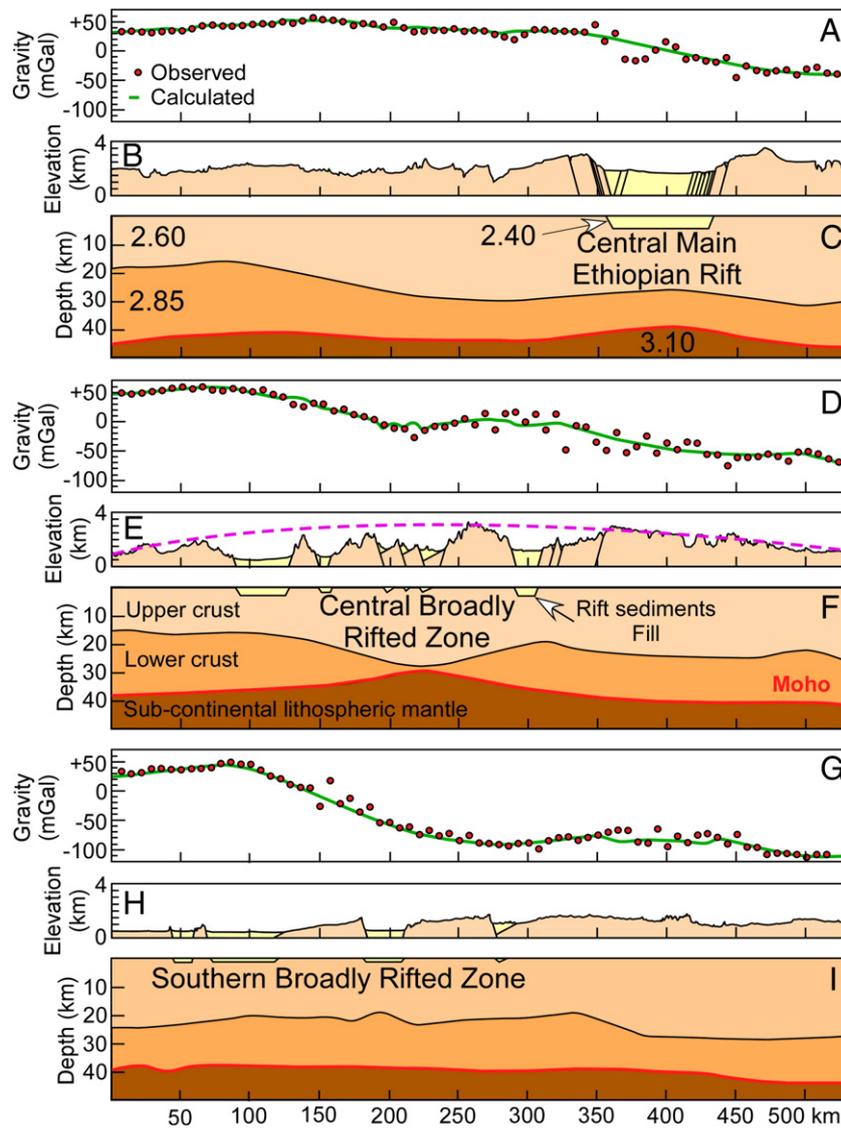
Fig. 9. (A), (B), and (C) observed Bouguer gravity anomaly extracted World Gravity Map (WGM 2012) along latitude 8°N extending between longitudes 35°E and 40°E (crossing the Central Main Ethiopian Rift), corresponding idealized cross-section, and best two-dimensional (2D) forward model to fit the observed Bouguer gravity anomaly. (D), (E) and (F) Same as above but along latitude 6°15′N (crossing the central Broadly Rifted Zone (BRZ)). (G), (H) and (I) Same as above but from along latitude 5°N (crossing the southern part of the BRZ). Numbers in panel C indicate densities in g/cm³. The pink line in panel E approximate the regional long wavelength doming associated with the BRZ. See Fig. 6 for location of the baselines of the models.

The 2D forward gravity model along latitude 6° 15′ N (central part of the BRZ; Fig. 9D and F) shows high sensitivity level to density variation at its central part (Fig. 10B). The calculated gravity anomaly of the lower crust changed from ~7 mGal to ~70 mGal as the density of this layer was changed from 2.80 g/cm³ to 3.02 g/cm³. Similarly, changing the density of the SCLM from 3.00 g/cm³ to 3.30 g/cm³ results in changing the calculated gravity anomaly from ~54 mGal to ~90 mGal (Fig. 10B). These significant variations indicate that the lower crust and the SCLM need to be better constrained more than the upper crust, which shows relatively lower sensitivity to density variation (Fig. 10B). Regardless, the Moho depth estimated from the 2D forward gravity model is in good agreement with that obtained from the 2D radially-averaged spectral analysis.

The 2D forward gravity model along latitude 5° N (southern part of the BRZ; Fig. 9G and I) shows medium to high level of sensitivity to density variation along its entire length, especially for the upper and lower crust in the western side of the model (Fig. 10C). For example, changing the density of the upper crust from its lower limit of 2.60 g/cm³ to its upper limit of 2.74 g/cm³ results in changing the

calculated gravity anomaly from ~−40 mGal to ~30 mGal (Fig. 10C). Also, changing the density of the lower crust from the lower limit (2.80 g/cm³) to the upper limit (3.02 g/cm³) results in increasing the calculated gravity anomaly from ~20 mGal to 100 mGal. Accordingly, this work gave emphasis to structures with high level of sensitivity and better constrained regions where there is a considerable shift in the calculated gravity anomaly as a response to density change.

The Bouguer gravity anomaly profiles across the Central Main Ethiopian Rift, (Fig. 9A), central part of the BRZ (Fig. 9D), and the southern part of the BRZ (Fig. 9G) do not suggest the presence of magmatic under-plating beneath these extensional structures. This is because of the lack of a high Bouguer gravity anomaly that can be interpreted as due to the presence of denser material such as magmatic under-plating. For example, the central part of the Bouguer gravity anomaly profile that crosses the central part of the BRZ is characterized by a low Bouguer gravity anomaly (Fig. 9 D). In addition, the density variation sensitivity analysis shows that increasing the density of the lower crust or the SCLM in this profile will result in significant increase of

Table 1
Comparison between Moho depth estimates for the Broadly Rifted Zone (BRZ) obtained from the two-dimensional (2D) radially-averaged power spectral analysis of of the World Gravity map (WGM 2012) and those obtained by Dugda et al. (2005) and Keranen et al. (2009) from passive seismic studies. Moho depth values are in km. Station locations are shown in Fig. 8A.

Location	This study	Dugda et al. (2005)	Keranen et al. (2009)	Difference between this study and Dugda et al. (2005)	Difference between this study and Keranen et al. (2009)
ADEE	39.0		38.0		1.0
ADUE	38.0		33.0		5.0
ARBA	32.5	30.0	28.0	2.5	4.5
AMME	38.0		38.0		0.0
BELA	38.0	38.0	40.5	0.0	−2.5
CHEF	38.5	37.0	33.0	1.5	5.5
DELE	36.5	36.0	35.5	0.5	1.0
DIKE	39.0		40.5		−1.5
GOBA	40.5	42.0	40.5	−1.5	0.0
HERO	38.5	42.0		−3.5	
JIMA	33.5	36.0	35.5	−2.5	−2.0
LEME	39.0		33.0		6.0
NAZA	36.5	27.0	35.5	9.5	1.0
SELA	38.5	27.0	40.5	11.5	−2.0
TERC	34.0	34.0	33.0	0.0	1.0
WELK	38.0	33.0		5.0	

the calculated gravity anomaly that is not matching the observed Bouguer gravity anomaly (Fig. 10B).

5. Discussion

5.1. Gravitational collapse and extension of a dynamic topography as a possible mechanism for the evolution of the Broadly Rifted Zone (BRZ)

Current models suggested for the BRZ largely considered it to represent an overlap zone between the southward propagating Southern Main Ethiopian Rift and the northward propagating and eastward migrating Kenya-Turkana Rift with possible modification through oblique extension, poly-phase rifting and anti-clockwise rotation of the Somalia Plate (Cerling and Powers, 1977; Moore and Davidson, 1978; WoldeGabriel and Aronson, 1987, 1991; Ebinger et al., 1993, 2000; Boccaletti et al., 1998; Bonini et al., 2005; Corti, 2009; Corti et al., 2013; Plilippon et al., 2014). These models predict younging in the age of the onset of extensional deformation from north to south in the Southern Main Ethiopian Rift and from south to north in the Kenya-Turkana Rift as well as progressive abandonment of faults activity within the BRZ from west to east. However, recent geochronological studies questioned these assumptions. For example, Balestrieri et al. (2016) reported ages ranging between 12 Ma and 10–8 Ma for the onset of rifting in the Gofa Province Basins in the central part of the BRZ and the Amaro Horst in the southeastern part of the BRZ (Fig. 3). This suggests rapid shift of tectonic activity in the BRZ from its northwestern part to its southeastern part. Additionally, Balestrieri et al. (2016) proposed that the onset of extension in the Gofa Province Basins and the Northern Main Ethiopian rift occurred at the same time as a result of ~11 Ma activities associated with reorganization of relative movement between the Nubia and Somalia Plates.

This work proposes a model for the evolution of the Ethiopian segment of the BRZ that advocates for its formation through multi-directional extension associated with gravitational collapse of the dynamic topography that formed at the southwestern margin of the Ethiopia-Yemen Plateau. This dynamic topography was developed due to uplift resulting from upwelling and ascendance of the asthenosphere beneath the BRZ. This model requires that thinning of the crust is accompanied by thinning of the SCLM beneath the BRZ. This work showed that considerable crustal thinning occurred beneath the BRZ (Fig. 8A and B). Additionally, Dugda et al. (2007) used joint inversion of the Rayleigh wave group velocities and receiver function to show that there is a broad thinning of the lithosphere beneath the Ethiopian Plateau and the Main Ethiopian Rift. Dugda et al. (2007) calculated that the SCLM
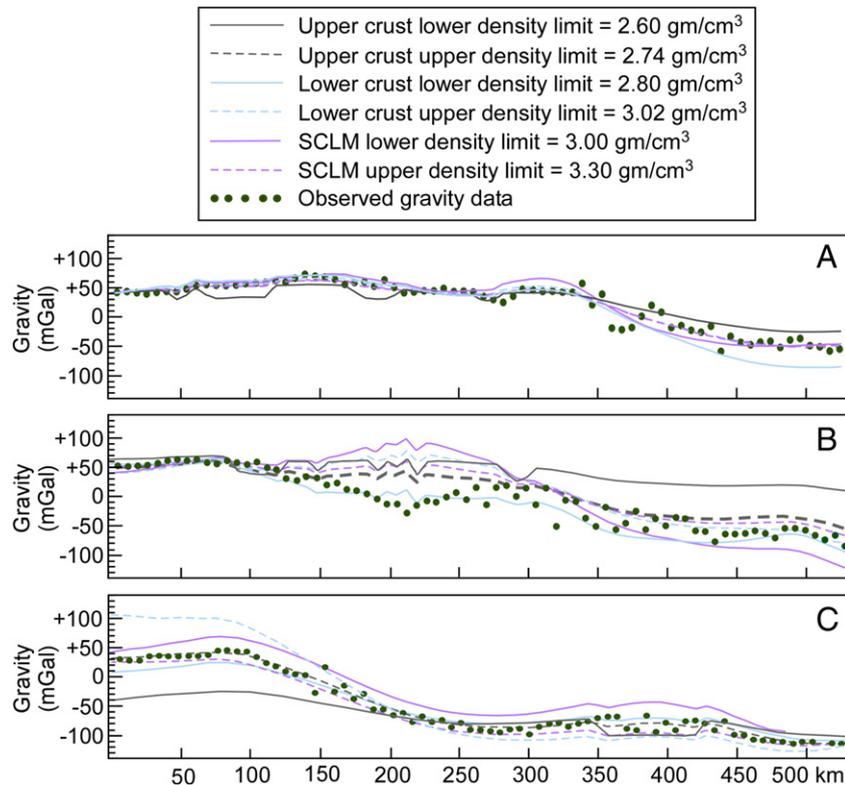

Fig. 10. Density variation sensitivity analysis of the two-dimensional (2D) forward gravity models presented in Fig. 9 along latitudes: (A) 8°N (crossing the Central Main Ethiopian Rift). (B) 6°15′N (crossing the central part of the Broadly Rifted Zone (BRZ)). (C) 5°N (crossing the southern part of the BRZ).

beneath the Main Ethiopian Rift has a slower shear wave velocity (4.1–4.2 km/s) compared to the Ethiopian Plateau (4.3 km/s) and that this slower velocity extends to a depth of 50 km (the SCLM depth). Dugda et al. (2007) suggested that 45–65% of the uplift in the Ethiopian Plateau can be attributed to lithospheric thinning during rifting which was caused by uprising of a mantle plume.

Gravitational collapse has been dominantly associated with relaxation of a crust that was thickened during an orogenic event. However, this work follows the general definition of Rey et al. (2001) which defines gravitational collapse as "gravity-driven ductile flow that effectively reduces lateral contrasts in gravitational potential energy". Rey et al. (2001) suggested that the flow of the lower crust away from the "deformed lithosphere" will results in thinning of the initially thickened crust. Rey et al. (2001) pointed to that gravitational collapse does not have to be accompanied by horizontal surface extension that is accommodated in the form of brittle deformation of the upper crust. Nonetheless, it is often the case that gravitational collapse through ductile flow of the lower crust will be accompanied by horizontal surface extension. For example, Tirel et al. (2004) found from the inversion of gravity data covering the Aegean domain (eastern Greece, western Turkey, Crete, and Aegean Sea) that the crust beneath the northern and southern parts of the domain is only 24–22 km thick. Tirel et al. (2004) attributed the presence of thin crust beneath this domain (which is characterized by the presence of metamorphic core complexes and multi-directional brittle rider faults) to middle Miocene gravitational collapse that resulted in thinning of the crust from 50 km to 25 km.

Asthenospheric upwelling beneath the BRZ is supported by S-wave seismic tomography results (Grand, 2002; Fishwick, 2010). This work outlines observations from S-wave velocity anomaly images at depths of 0–100 km, 100–175 km, 175–250 km, and 250–325 km beneath the BRZ and its surroundings from the Grand (2002) model (Figs. 11 and 12). It also outlines observations from S-wave velocity anomaly images at depth range of 75 km, 100 km, 125 km, and 150 km from Fishwick et al. (2010) model (Fig. 13).
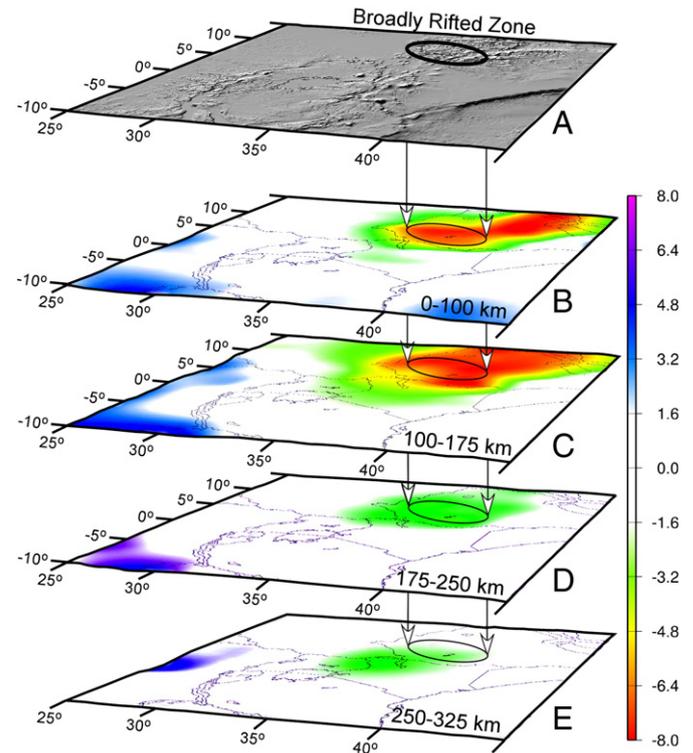

Fig. 12. Three-dimensional (3D) perspective views of the surface expression of the Broadly Rifted Zone (BRZ) and its surroundings from Global Topographic 30 arc second (GTOPO30) Digital Elevation Model (DEM) and underlying S-wave velocity seismic tomography slices at depth of 0–100 km, 100–175 km, 175–250 km, and 250–325 km. The seismic data are from the model of Grand (2002). Color bar shows S-wave velocity anomaly in percent relative to the Primary Reference Earth Model (PREM).
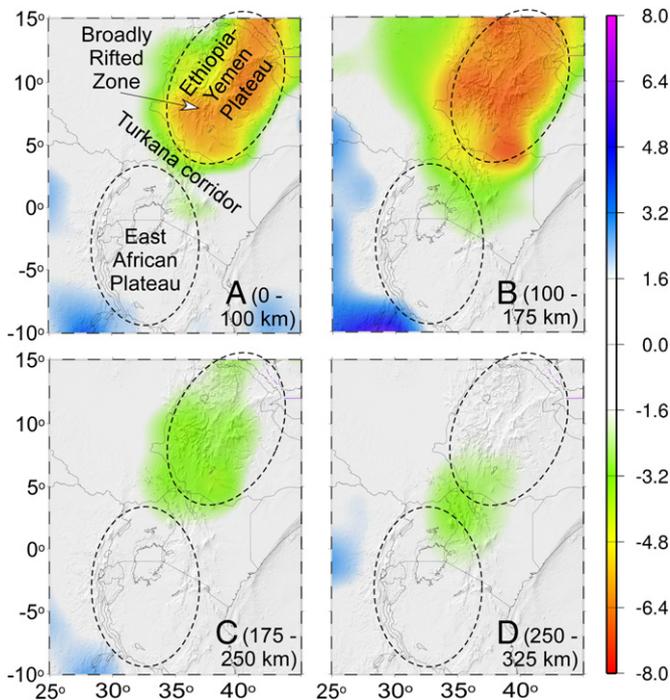

Fig. 11. Horizontal S-wave velocity seismic tomography slices from beneath the Broadly Rifted Zone (BRZ) and its surroundings at 0–100 km depth (A), 100–175 km depth (B), 175–250 km depth (C) and 250–325 km depth (D). The seismic data are from the model of Grand (2002). Color bar shows S-wave velocity anomaly in percent relative to the Primary Reference Earth Model (PREM).

The S-wave velocity seismic tomography depth slices extracted from the model of Grand (2002) show NE-SW elongated zones of slower S-wave velocity anomaly relative to the Primary Reference Earth Model (PREM) at depths of 0–100 km and 100–175 km (Fig. 12A and B). This anomaly is ~1000 km in width and the S-wave velocity in its central part is ~8% slower relative to PREM (Fig. 12A and B). This anomaly underlies much of the Ethiopia-Yemen Plateau and it does not appear to extend southwest-ward beyond the Turkana Topographic Corridor (Figs. 12A, and B, and 13A–C). At depth of 175–250 km the slower S-wave velocity anomaly becomes blurred showing ~4% slower velocities relative to PREM (Figs. 12C and 13D). At this depth, the S-wave velocity anomaly seems to be centered beneath the southwestern part of the Ethiopia-Yemen Plateau (Fig. 12C). At 250–325 km depth the position of the slower S-wave velocity anomaly shifts to the southwest and appears to be centered beneath the southern part of the Ethiopia-Yemen Plateau, the Turkana Topographic Corridor and the northern-most part of the East African Plateau (Figs. 12D and 13E).

The S-wave seismic tomography depth slices extracted from the Fishwick et al. (2010) model are similar to those obtained from Grand (2002) model (Fig. 13). The only difference is that the slower S-wave velocity anomalies seems to extend northwest-ward, but not with the same difference in S-wave velocity relative to the International Association of Seismology and the Physics of the Earth (IASP91) model as that of the anomaly that is elongated in a NE-SW direction (Fig. 12). The 75 km and 100 km depth slices show the slower S-wave velocity anomaly beneath the Ethiopia-Yemen Plateau extending from around the Turkana Topographic Corridor northeast-ward to the Afar Depression where these anomalies are up to ~8% slower than the IASP91 model (Fig. 13A and B). The difference between the slower S-wave velocity anomaly and the IASP91 model decreases at 125 km and 150 km
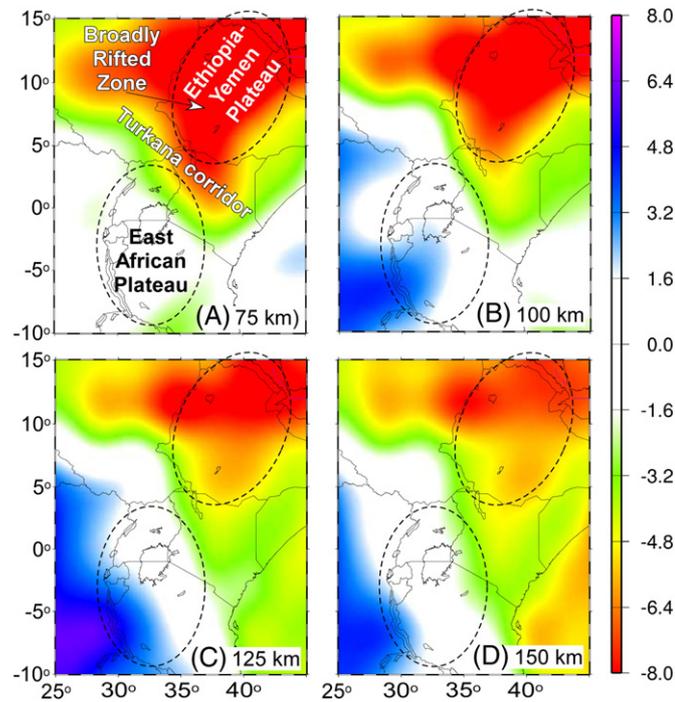
Fig. 13. S-wave velocity anomaly slices based on Fishwick (2010) model at depth of: (A) 75 km. (B) 100 km. (C) 125 km. (D) 150 km. Color bar shows S-wave velocity anomaly in percent relative to the International Association of Seismology and the Physics of the Earth Interior (IASP91) model.

depth, but shows the same pattern extending from the Turkana Topographic Corridor to the Afar Depression (Fig. 13C and D).

Fig. 14 illustrates the evolution of the BRZ in relationship to a NE-flowing mantle flow rising from beneath the southern part of the Ethiopia-Yemen Plateau. Beside the geochronological and seismic tomography observations discussed above, additional morpho-tectonic, geometrical, kinematics, and mantle dynamics observations are discussed below in support of this model.

5.2. Morpho-tectonic, geometrical and kinematics observation

The formation of the BRZ through gravitational collapse of a dynamic topography agrees with the uplift model proposed by Gani et al. (2007) for the Northwestern Ethiopian Plateau. From quantitative geomorphologic analysis, Gani et al. (2007) documented three incision phases between 29 and 10 Ma, 10 and 6 Ma, and 6 Ma to present. Gani et al. (2007) also documented significant increase of the rate of the incision of the Blue Nile between 10 and 6 Ma and 6 Ma and present. Gani et al. (2007) attributed the increase of the rate of incision to pulsed plateau uplift caused by ponded mantle plume material beneath the Ethiopian Plateau.

The association of the formation of the BRZ with a NE-flowing mantle flow rising from beneath the southern part of the Ethiopia-Yemen Plateau reconciles with the presence of the Turkana Topographic Corridor between the Ethiopia-Yemen and East African plateaus. The presence of this topographic corridor indicates that the two dynamic topography regions were uplifted from the upwelling of two distinct asthenospheric sources. If the dynamic topography of the two plateaus was formed from a single upwelling asthenospheric source, then this will result in a single continuous uplifted terrain without the presence of a topographic break such as the Turkana Topographic Corridor.

Within the Ethiopia-Yemen Plateau, the BRZ is characterized by the presence of a broad (~500 km wide) domical uplift within which

extensional structures were superimposed (Fig. 9E). Philippon et al. (2014) conducted morpho-tectonic analysis in the three basins constituting the Gofa Province Basins (Swala, Beto and Mati Dancha) and the Chew Bahir Basin (Fig. 3) by calculating the normalized steepness index (K_{sn}) and the concavity (θ) of the longitudinal profiles of rivers draining these basins. Philippon et al. (2014) found that the rivers draining the two northwestern basins of the Gofa Province Basins (Swala and Beto) have higher "θ" values than the rivers draining the southeastern basin (Mati Dancha) that in turn has higher "θ" values than the rivers draining the Chew Bahir Basin. This suggests southward decrease in the maturity of these rivers which in turn suggests a history of southward migration of rock uplift and tectonic activity. This is because, although this work suggested that the mantle flow migrates from south to north, it is expected that the youngest topography to be above the source of the asthenospheric upwelling feeding the flow. Additionally, Philippon et al. (2014) found that the western part of the Chew Bahir Basin has higher "K_{sn}" values compared to its eastern part suggesting higher rock uplift in the west. This morpho-tectonic pattern is unlikely to develop from rift flank uplift of rift footwalls represented by the Northwestern and Southeastern Ethiopian plateaus Rather, such pattern is better reconciled with broad central uplift of the BRZ.

Although the rift basins constituting the BRZ are either N or NE-trending (Fig. 3), NW-trending extensional structures are also apparent (Fig. 3). These are particularly obvious in the transitional region between the Gofa Province Basins and the Chew Bahir Basin (Fig. 3). Additionally, the border faults of many of the rift basins constituting the BRZ show zig-zag pattern resulting from alternation of shorter segments of the border faults from NE-trending to NW-trending. This is best exemplified by the western border fault of the Chew Bahir Basin (Fig. 3). Kinematic analysis of normal faults in the Chencha Horst (Fig. 3) by Bonini et al. (2005) suggests a change in extension within the BRZ from NNE-SSW to E-W to NW-SE to E-W. This change in extension direction has been interpreted as multi-phase deformation arising from clockwise rotation of the Somalia Plate (Bonini et al., 2005). However, in absence of precise age dating indicating that these different extensional events occurred in different times coupled with the presence of N, NE and NW-trending extensional structures within the BRZ, synchronous multi-directional extension triggered by gravitational collapse remains a possibility for the BRZ.

5.3. Mantle dynamics observations

The dynamic topography of the Ethiopia-Yemen and East African plateaus that is associated with the Northern, Eastern and Western branches of the EARS has been attributed to asthenospheric upwelling. However, there have been competing ideas regarding the mantle plumes dynamics and sources. For example, Ebinger and Sleep (1998) suggested the presence of a single mantle plume beneath the stationary African Plate with lateral flow and ponding. Alternatively, Rogers et al., (2000) have argued for the presence of two distinct mantle plumes; Afar Mantle Plume beneath the Ethiopian-Yemen Plateau and the Kenya Mantle Plume beneath the East African Plateau. On the other hand, Moucha and Forte (2011) suggested that the dynamic topography of the Northern, Eastern and Western branches of the EARS was produced by northward movement of the African Plate over the upwelling African Super Plume.

The model proposed in this work for the evolution of the BRZ better reconciles with the suggestion that the origin of the dynamic topography of the Ethiopia-Yemen Plateau was due to a mantle flow that rises from the southern part of the dome before flowing NE-ward beneath the Main Ethiopian Rift and the Afar Depression. This suggestion is supported by results from S-wave splitting that show the fast splitting time beneath the Main Ethiopian Rift and the Afar Depression is in northeast direction (Gao et al., 2010). Gao et al. (2010) interpreted this S-wave splitting pattern to originate from a deeper source represented by a NE-flowing mantle flow and a shallower source represented by NE-
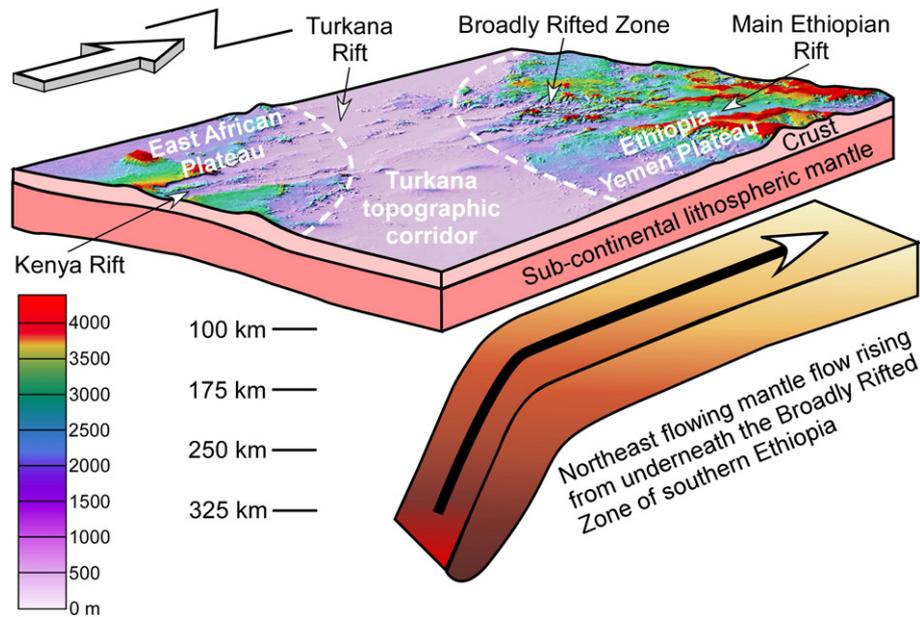
Fig. 14. Conceptual three-dimensional (3D) model illustrating the association of the Broadly Rifted Zone (BRZ) with a mantle upwelling rising from beneath the BRZ and becoming a NE-flowing mantle flow at shallow depth. The Digital Elevation Model (DEM) is extracted from Shuttle Radar Topography Mission (SRTM) data.

oriented magmatic segments. Further north, Daradich et al. (2003) used viscous-flow simulation to suggest that the asymmetrical dynamic topography of the Red Sea (higher elevation in its eastern margin compared to the western margin) and the eastward tilting of the Arabian Plate was related to N-flowing mantle flow. Hansen et al. (2006) found, from S-wave splitting study that the fast splitting time in the Arabian Plate, specially its western margin, is in a N-S direction. Hansen et al. (2006) explained the fast S-wave splitting direction as due to northward motion of the Arabian Plate combined with "asthenospheric density-driven flow".

6. Conclusions

Results from imaging the Moho depth using 2D radially-averaged power spectral analysis and 2D forward modeling of the WGM 2012, and observations from S-wave seismic tomography images of the SCLM and asthenosphere beneath the ~315 km wide BRZ and its surroundings within the EARS in southern Ethiopia suggest: (1) elevated Moho beneath the BRZ forming a domical geometry, and (2) slower NE-SW trending S-wave velocity anomaly beneath the BRZ, the Main Ethiopian Rift and the Afar Depression at 75–150 km depth. This anomaly becomes elliptical in shape and shifts to the southwest at 175–250 km depth centered beneath the BRZ. This elliptical anomaly shifts further southwest at 250–325 km depth centered beneath the southern part of the Ethiopia-Yemen Plateau, the Turkana Topographic Corridor, and the northern part of the East African Plateau. These observations, together with morphological observation (broad long wavelength topographic doming), and normal fault geometry and kinematics suggestive of synchronous multi-directional extension were used to propose that the BRZ was formed as a result of gravitation collapse of a dynamic topography created by a NE-flowing mantle flow that is rising from the southern part of the Ethiopia-Yemen Plateau.

References

Abebe, B., Acocella, V., Korme, T., Ayalew, D., 2007. Quaternary faulting and volcanism in the Main Ethiopian Rift. J. Afr. Earth Sci. 48, 115–124.

Balestrieri, M.L., Bonini, M., Corti, G., Sani, F., Phillippon, M., 2016. A refinement of the chronology of rift-related faulting in the Broadly Rifted Zone, southern Ethiopia, through apatite fission-track analysis. Tectonophysics 671, 42–55.

Boccaletti, M., Bonini, M., Mazzuoli, R., Abebe, B., Piccardi, L., Tortorici, L., 1998. Quaternary oblique extensional tectonics in the Ethiopian Rift (Horn of Africa). Tectonophysics 287, 97–116.

Bonini, M., Corti, G., Innocenti, F., Manetti, P., Mazzarini, F., Abebe, T., Pecskay, Z., 2005. Evolution of the Main Ethiopian Rift in the frame of Afar and Kenya rifts propagation. Tectonics 24, TC1007. http://dx.doi.org/10.1029/2004TC001680.

Bonvalot, S., Balmino, G., Briais, A., M. Kuhn, Peyrefitte, A., Vales, Biancale, R., Gabalda, G., Moreaux, G., Reinquin, F., Sarrailh, M., 2012. World Gravity Map, 1:50,000,000. Editors: Bureau Gravimetrique International (BGI) – Commission for the Geological Map of the World (CGMW), Centre National d'Etudes Spatiales (CNES) – Institut de Reserche pour le Development (IRD), Paris.

Cerling, T.E., Powers, D.W., 1977. Paleorifting between the Gregory and Ethiopian Rifts. Geology 5, 441–444.

Chorowicz, J., 2005. The East African Rift System. J. Afr. Earth Sci. 43, 379–410.

Chu, D., Gordon, R., 1999. Evidence for motion between Nubia and Somalia along the southwest Indian ridge. Nature 398, 64–67.

Corti, G., 2009. Continental rift evolution: from rift initiation to incipient break-up in the Main Ethiopian Rift, East Africa. Earth Sci. Rev. 96, 1–53.

Corti, G., Sani, F., Philippon, M., Sokoutis, D., Willingshofer, E., Molin, P., 2013. Quaternary volcano-tectonic activity in the Soddo region, western margin of southern Main Ethiopian Rift. Tectonics 32, 861–879.

Daradich, A., Mitrovica, J.X., Pysklywec, R.N., Willett, S.D., Forte, A.M., 2003. Mantle flow, dynamic topography, and rift-flank uplift of Arabia. Geology 31, 901–904.

Dugda, M.T., Nyblade, A.A., Julia, J., Langston, C.A., Ammon, C.J., Simiyu, S., 2005. Crustal structure in Ethiopia and Kenya from receiver function analysis: implications for rift development in eastern Africa. J. Geophys. Res. Solid Earth 110, B01303. http://dx.doi.org/10.1029/2004JB003065.

Dugda, M.T., Nyblade, A.A., Julia, J., 2007. Thin lithosphere beneath the Ethiopian Plateau revealed by a joint inversion of Rayleigh wave group velocities and receiver functions. J. Geophys. Res. Solid Earth 112, B08305. http://dx.doi.org/10.1029/2006JB004918.

Ebinger, C.J., Casey, M., 2001. Continental breakup in magmatic provinces: an Ethiopian example. Geology 29, 527–530.

Ebinger, C.J., Hayward, N.J., 1996. Soft plates and hot spots: views from afar. J. Geophys. Res. Solid Earth 101, 21,859–21,876.

Ebinger, C.J., Sleep, N.H., 1998. Cenozoic magmatism in central and east Africa resulting from impact of one large plume. Nature 395, 788–791.

Ebinger, C.J., Yemane, T., WoldeGabriel, G., Aronson, J.L., Walter, R.C., 1993. Late Eocene — recent volcanism and faulting in the southern Main Ethiopian Rift. J. Geol. Soc. Lond. 150, 99–108.

Ebinger, C.J., Yemane, T., Harding, D.J., Tesfaye, S., Kelley, S., Rex, D.C., 2000. Rift deflection, migration, and propagation: linkage of the Ethiopian and Eastern rifts, Africa. Geol. Soc. Am. Bull. 112, 163–176.

Fishwick, S., 2010. Surface wave tomography: imaging of the lithosphere-asthenosphere boundary beneath central and southern Africa? Lithos 120, 63–73.

Gani, N.D.S., Gani, M.R., Abdelsalam, M.G., 2007. Blue Nile incision on the Ethiopian Plateau: pulsed plateau growth, Pliocene uplift, and hominin evolution. 2007. GSA Today 17, 4–11.

Gao, S.S., Liu, K.H., Abdelsalam, M.G., 2010. Seismic anisotropy beneath the Afar Depression and adjacent areas: implications for mantle flow. J. Geophys. Res. Solid Earth 115, B12330. http://dx.doi.org/10.1029/2009JB007141.

Grand, S.P., 2002. Mantle shear-wave tomography and the fate of subducted slabs. Philosophical Transactions - Royal Society. Mathematical. Phys. Eng. Sci. 360, 2475–2491.

Hansen, S., Schwartz, S., Al-Amri, A., Rodgers, A., 2006. Combined plate motion and density-driven flow in the asthenosphere beneath Saudi Arabia: evidence from shear-wave splitting and seismic anisotropy. Geology 34, 869–872.

Hayward, N.J., Ebinger, C.J., 1996. Variations in the along-axis segmentation of the Afar Rift System. Tectonics 15, 244–257.

Hendrie, D.B., Kusznir, N.J., Morley, C.K., Ebinger, C.J., 1994. Cenozoic extension in northern Kenya: a quantitative model of rift basin development in the Turkana region. Tectonophysics 236, 409–438.

Keranen, K.M., Klemperer, S.L., Julia, J., Lawrence, J.F., Nyblade, A.A., 2009. Low lower crustal velocity across Ethiopia: is the Main Ethiopian Rift a narrow rift in a hot craton? Geochem. Geophys. Geosyst. 10, Q0AB01. http://dx.doi.org/10.1029/2008GC002293.

Leseane, K., Atekwana, E.A., Mickus, K.L., Abdelsalam, M.G., Shemang, E.M., Atekwana, E.A., 2015. Thermal perturbations beneath the incipient Okavango Rift Zone, northwest Botswana. J. Geophys. Res. Solid Earth 120, 1210–1228.

Levitte, D., Columba, J., Mohr, P., 1974. Reconnaissance Geology of the Amaro Horst, Southern Ethiopian Rift. Geol. Soc. Am. Bull. 85, 417–422.

Mackenzie, G.D., Thybo, H., Maguire, P.K.H., 2005. Crustal velocity structure across the Main Ethiopian Rift: results from 2-dimensional wide-angle seismic modeling. Geophys. J. Int. 162, 994–1006.

Mammo, T., 2012. Analysis of gravity field to reconstruct the structure of Omo basin in SW Ethiopia and implications for hydrocarbon potential. Mar. Pet. Geol. 29, 104–114.

Mengesha, T., Tadiwos, C., Workineh, H., 1996. Geological map of Ethiopia, 2nd edition. Bulletin of the Ethiopian Institute of Geological Survey, 3, scale 1:2.000.000, 1 sheet. OCLC: 46451457, Addis Ababa.

Moore, J.M., Davidson, A., 1978. Rift structure in southern Ethiopia. Tectonophysics 46, 159–173.

Moucha, R., Forte, A.M., 2011. Changes in African topography driven by mantle convection. Nat. Geosci. 4, 707–712.

Philippon, M., Corti, G., Sani, F., Bonini, M., Balestrieri, M.L., Molin, P., Cloetingh, S., 2014. Evolution, distribution, and characteristics of rifting in southern Ethiopia. Tectonics 33, 485–508.

Pik, R., Marty, B., Carignan, J., Yirgu, G., Ayalew, T., 2008. Timing of East African Rift development in southern Ethiopia: implication for mantle plume activity and evolution of topography. Geology 36, 167–170.

Rey, P., Vanderhaeghe, O., Teyssier, C., 2001. Gravitational collapse of the continental crust: definition, regimes and modes. Tectonophysics 342, 435–449.

Rogers, N., Macdonald, R., Fitton, J.G., George, R., Smith, M., Barreiro, B., 2000. Two mantle plumes beneath the East African rift system: Sr, Nd and Pb isotope evidence from Kenya Rift basalts. Earth Planet. Sci. Lett. 176, 387–400.

Saria, E., Calais, E., Stamps, D.S., Delvaux, D., Hartnady, C.J.H., 2014. Present-day kinematics of the East African Rift. J. Geophys. Res. Solid Earth 119, 3584–3600.

Stuart, G.W., Bastow, I.D., Ebinger, C.J., 2006. Crustal structure of the northern Main Ethiopian Rift from receiver function studies. Geol. Soc. Lond., Spec. Publ. 259, 253–267.

Talwani, M., Worzel, J.L., Landisman, M., 1959. Rapid gravity computations for two-dimensional bodies with application to the Mendocino submarine fracture zone. J. Geophys. Res. 641, 49–59.

Tiberi, C., Ebinger, C., Ballu, V., Stuart, G., Oluma, B., 2005. Inverse models of gravity data from the Red Sea-Aden-East African rifts triple junction zone. Geophys. J. Int. 163, 775–787.

Tirel, C., Gueydan, F., Tiberi, C., Brun, J.-P., 2004. Aegean crustal thickness inferred from gravity inversion. Geodynamic. Implications Earth Planet. Sci. Lett. 288, 267–280.

Tselentis, G.A., Drakopoulos, J., Dimitriadis, K., 1988. A spectral approach to Moho depths estimation from gravity measurements in Epirus (NW Greece). J. Phys. Earth 36, 255–266.

Vetel, W., Le Gall, B., 2006. Dynamics of prolonged continental extension in magmatic rifts: the Turkana Rift case study (North Kenya). Geol. Soc. Lond., Spec. Publ. 259, 209–233.

Vétel, W., Le Gall, B., Walsh, J.J., 2005. Geometry and growth of an inner rift fault pattern: the Kino Sogo Fault Belt, Turkana Rift (North Kenya). J. Struct. Geol. 27, 2204–2222.

WoldeGabriel, G., Aronson, J.L., 1987. Chow Bahir rift: a "failed" rift in southern Ethiopia. Geology 15, 430–433.

WoldeGabriel, G., Yemane, T., White, T., Asfaw, B., Suwa, G., 1991. Age of volcanism and fossil in the Burji-Soyoma area, Amaro Horst, southern Main Ethiopian Rift. J. Afr. Earth Sci. 13, 437–447.

Won, I.J., Bevis, M., 1987. Computing the gravitational and magnetic anomalies due to a polygon: algorithms and Fortran subroutines. Geophysics 52, 232–238.